Asymmetric impact of Central Pacific ENSO on the reduction of tropical cyclone genesis frequency over the western North Pacific since the late 1990s

Han-Kyoung Kim[1] · Kyong-Hwan Seo[2] · Sang-Wook Yeh[3] · Nam-Young Kang[4,5] · Byung-Kwon Moon[1]

Abstract

Tropical cyclone (TC) genesis frequency over the western North Pacific (WNP) is significantly reduced since the late 1990s, coinciding with a Pacific decadal oscillation (PDO) phase transition from positive to negative. In this study, the underlying mechanism for this change is investigated through analysis of asymmetric central Pacific (CP) El Niño-Southern Oscillation (ENSO) properties induced by the negative PDO phase. Our results suggest that the significant reduction is caused by asymmetric CP ENSO properties, in which the CP La Niña is more frequent than the CP El Niño during negative PDO phases; furthermore, stronger CP La Niña occurs during a negative PDO phase than during a positive PDO phase. CP La Niña (El Niño) events generate an anticyclonic (cyclonic) Rossby wave response over the eastern WNP, leading to a significant decrease (increase) in eastern WNP TC genesis. Therefore, more frequent CP La Niña events and the less frequent CP El Niño events reduce the eastern WNP mean TC genesis frequency during a negative PDO phase. In addition, stronger CP La Niña events during a negative PDO phase reinforce the reduction in eastern WNP TC genesis. The dependency of CP ENSO properties on the PDO phase is confirmed using a long-term climate model simulation, which supports our observational results. Our results will also improve understanding of TC in other basins, since both PDO and CP ENSO variability influence global dynamics.

Keywords Tropical cyclone · Pacific decadal oscillation · Central Pacific El Niño-Southern oscillation

1 Introduction

Despite their destructive properties, tropical cyclones (TCs) are necessary to regulate Earth's energy balance between equatorial and higher latitudes. The western North Pacific (WNP) is one of the most active basins for TC genesis,

averaging ~ 19 TCs annually during the last three decades (i.e., 1979–2013) and accounting for one third of global TC development (Kim and Seo 2016). Therefore, an improved understanding of TC activity (i.e., frequency, track, and intensity) in this basin is imperative for helping mitigate the damage caused by their landfall.

The TC genesis frequency and location experience significant variations on intraseasonal, interannual, and decadal time scales because they are affected by large-scale atmospheric and oceanic variability, including intraseasonal oscillations (Li and Zhou 2013a, b; Kim and Seo 2016), the El Niño-Southern Oscillation (ENSO; Wang and Chan 2002; Camargo et al. 2007; Chen and Tam 2010; Kim and Seo 2016), interannual variation of Atlantic sea surface temperature (SST; Yu et al. 2016), western Pacific subtropical high (Wang et al. 2013a; Kim and Seo 2016), Pacific meridional mode (Zhang et al. 2016), Pacific decadal oscillation (PDO; Chan 2008; Liu and Chan 2013), and several other factors.

On the interannual time scale, the ENSO is the most crucial factor modulating TC genesis location over the WNP.

✉ Byung-Kwon Moon
  moonbk@jbnu.ac.kr

[1] Division of Science Education/Institute of Fusion Science, Jeonbuk National University, Jeonju, South Korea

[2] Department of Atmospheric Sciences, Division of Earth Environmental System, Pusan National University, Busan, South Korea

[3] Marine Sciences and Convergent Technology, ERICA, Hanyang University, Ansan, South Korea

[4] National Typhoon Center, Korea Meteorological Administration, Jeju, South Korea

[5] Department of Geography, College of Social Sciences, Kyungpook National University, Daegu, South Korea

For example, Wang and Chan (2002) used the Niño-3.4 index to show that TC genesis increases in the southeast quadrant of the WNP during El Niño years and decreases in the same quadrant during La Niña years. They also found that the resulting TCs are characterized by stronger intensity and longer lifespan in El Niño years as compared with La Niña years.

The ENSO can be divided into two types: an eastern Pacific (EP) ENSO, with an SST variation center located in the EP, and a central Pacific (CP) ENSO, with an SST variation center located in the CP. These have different characteristics in terms of spatial structure, underlying dynamic mechanisms, temporal evolution, and teleconnection patterns (Kao and Yu 2009; Jin et al. 2013; Yeh et al. 2018). From this perspective, previous studies have demonstrated different roles for the two types of ENSOs in the frequency of TC genesis in the WNP (Chen and Tam 2010; Yeh et al. 2010; Wang et al. 2013b; Kim and Seo 2016) and intensification of the relationship between the CP ENSO and WNP TC genesis frequency (Liu and Chen 2018; Zhao and Wang 2019). Kim and Seo (2016) showed that the EP El Niño leads to a significant decrease (~40%) in TC genesis in the western part of the WNP through a reversed Walker circulation with downward motion. Conversely, the CP El Niño generates a cyclonic Rossby wave response over the northwest of the SST forcing, resulting in a significant increase (~50%) in TC genesis over the eastern part of the WNP. Chen and Tam (2010) examined the different relationships between WNP TC genesis frequency and CP/EP ENSO. They showed that the TC genesis frequency is significantly positively correlated with the CP ENSO because the heating source (sink) of CP El Niño (La Niña) generates large-scale cyclonic (anticyclonic) circulation over the WNP. In contrast, the EP ENSO negatively (positively) correlates with TC genesis frequency over the northern (southeastern) part of the WNP. That is due to the anticyclonic (cyclonic) circulation associated with the heating sink (source) over the northern (southeastern) part of the WNP, resulting in a decrease (increase) in TC genesis frequency during EP El Niña years, while for La Niña years, the reverse may be true.

Previous studies on long-term climate variabilities have shown a significant reduction of TC genesis frequency during various seasons (Chan 2008; Liu and Chan 2013; Hsu et al. 2014; Choi et al. 2015; He et al. 2015; Zhao and Wang 2016; Zhang et al. 2018; Zhao and Wang 2019) and its associated increase of ratio intensification of TCs (Zhao et al. 2018) over the WNP since the late 1990s. For instance, Liu and Chan (2013) investigated the recently inactive period (i.e., 1998–2011) of TC activity and found that it resulted from strong vertical wind shear and a strong subtropical high. Zhang et al. (2018) used observations and high-resolution climate model experiments to suggest that the decadal variation of the Atlantic multidecadal oscillation (AMO) and PDO cause intensified vertical wind shear in the southeastern WNP, leading to a decrease in TC genesis frequency since the late 1990s.

It is interesting to note that the PDO and the ENSO, which are modulation factors of TC genesis frequency, interact with each other. From this point of view, Lin et al. (2018) applied statistical analysis from observations and 19 Coupled Model Intercomparison Project Phase 5 (CMIP5) models to demonstrate that the PDO can modulate the asymmetric frequency of the ENSO. El Niño events occur three times more often than La Niña events in positive PDO phases while dropping to approximately half the number of La Niña events during negative PDO phases (An 2018).

Analysis of observations shows that the PDO phase changed from positive to negative around 1997/8. Concurrently, the TC genesis frequency over the WNP significantly decreased by 19% compared with both PDO phases and its reduction mainly comes from the eastern WNP. Although previous studies have shown that the significant reduction of TC genesis frequency mainly results from the intensification of vertical wind shear on a decadal time scale, the relationship between asymmetric CP ENSO properties and the reduction in WNP TC genesis frequency during negative PDO phases has not been studied.

Therefore, the purpose of this study is to reveal the underlying mechanism for the significant reduction of TC genesis frequency over the WNP since the late 1990s with reference to asymmetric CP ENSO properties induced by the negative PDO phase. We investigate the connection between them, adhering to the finding of Kim and Seo (2016) that large-scale atmospheric and oceanic variability (e.g., ENSO) influence WNP TC genesis frequency in sub-regions rather than across the whole WNP, proving that the significant overall reduction in TCs has mostly occurred within specific WNP sub-regions.

The remainder of the paper is organized as follows. Section 2 describes the datasets and regime shift algorithms used in this study. Section 3 presents the interdecadal variations in the PDO and WNP TC genesis frequency; in addition, the mechanisms connecting the significant reduction in WNP TC genesis frequency and asymmetric CP ENSO properties induced by the negative PDO phase are also presented. Summary and discussions are detailed in Sect. 4.

2 Data and methods

2.1 Observational data

This study utilizes the TC information dataset from the Regional Specialized Meteorological Centers-Tokyo Typhoon Center, which contains information on storm name, date, type, latitude and longitude, central pressure, and maximum sustained wind speed (V_{max}) at 6-h intervals. Typically,

TCs are categorized into three groups depending on their wind speed (V_{max}): tropical depression ($V_{max} < 17$) m s^{-1}, tropical storm (17 m s$^{-1} \leq V_{max} < 34$) m s^{-1}, and typhoon ($V_{max} \geq 34$) m s^{-1}. In this study, TCs are referred to as tropical storms and typhoons; as such, the genesis and decay location of each TC are selected as the first and last observed positions, respectively, with intensity greater than a tropical storm. The peak TC season in the WNP is defined as July–October (JASO), during which approximately 70% of TCs form.

To analyze the large-scale atmospheric and oceanic variability related to the TC genesis frequency, we use atmospheric datasets (e.g., geopotential height and wind) from the National Centers for Environmental Prediction-National Center for Atmospheric Research (NCEP-NCAR; Kalnay et al. 1996). We also use monthly mean SST from the Extended Reconstructed Sea Surface Temperature version 4 (ERSST v4; Huang et al. 2014; Liu et al. 2015) to analyze PDO and ENSO variability. Furthermore, we use the monthly PDO index provided by the University of Washington (http://research.jisao.washington.edu/pdo/PDO.latest.txt), which is calculated using the method of Mantua et al. (1997).

Moon et al. (2019) discussed the reliability of the TC dataset and showed that a geostationary satellite has been used to generate the TC dataset since 1982. In addition, in and after 2014, the PDO phase changed from negative to positive; therefore, we restricted our analysis period to 1982–2013.

2.2 Model simulation

To examine the impact of the PDO on asymmetric CP ENSO properties on a long-term time scale, we use the long-term unforced Community Climate System Model Version 3 (CCSM3), which is a fully coupled model including atmosphere (CAM3), land (CLM3), ocean (POP), and sea ice (CSIM) models. The experiment is conducted taking a duration of 600 years into account with a fixed CO_2 concentration of 355 ppmv and utilizing simulated data for the last 500 years; detailed descriptions of this model can be found in Collins et al. (2006).

## 2.3 Rodionov regime shift algorithm

The Rodionov regime shift algorithm is used to detect interdecadal regime shifts in an interannual time series. The algorithm identifies significant interdecadal change points in sequential running means with a set cut-off length and at a confidence level based on the Student's t test. If the difference between two adjacent sequential running means during a certain cut-off period is statistically significant, then a regime shift is detected. More detailed information on this algorithm can be found in Rodionov (2004).

3 Results

3.1 Interdecadal variation of PDO and typhoon genesis frequency

When the Rodionov regime shift algorithm with a cut-off length of 10 years and at a 90% confidence level is applied to the interannual time series of the JASO mean PDO from 1982 to 2013, a clear interdecadal change point appears around 1997/98 (black solid line in Fig. 1). Thus, the entire analysis period (1982–2013) can be divided into two subperiods based on the dominant PDO phase: the positive (1982–1997, P1) and negative (1998–2013, P2) sub-periods. The positive PDO phase is defined as cold SST anomalies in the mid latitude northwestern Pacific and warm SST

Fig. 1 Interannual time series of the July–October mean PDO (black line) and TC genesis frequency over the WNP during the positive PDO (P1: 1982–1997; red line) and negative PDO (P2: 1988–2013; blue line) periods. The Rodionov regime shift algorithm is applied to detect the interdecadal change point

PDO index and TC genesis frequency
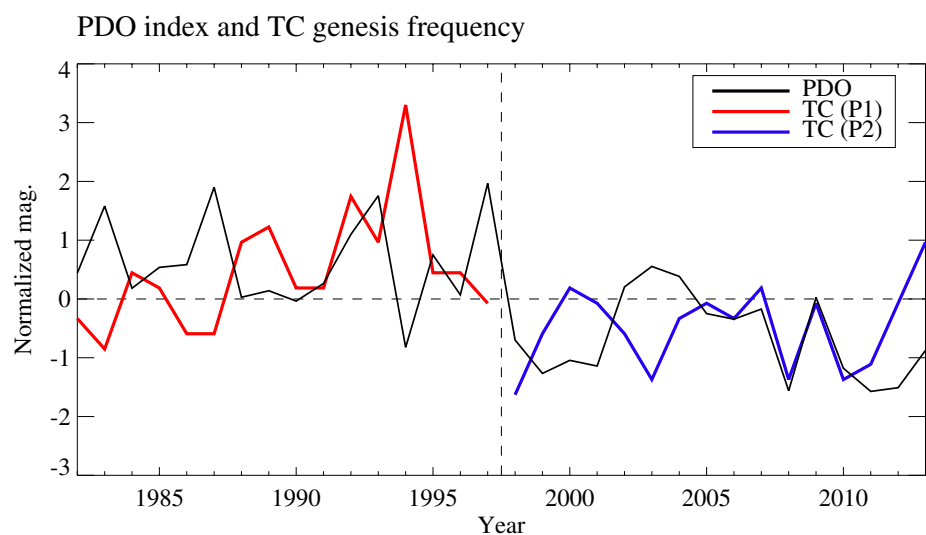
anomalies over the central Pacific, and vice versa for the negative PDO phase (Mantua et al. 1997). The year-to-year TC genesis frequency over the WNP had a similar interdecadal change point based on the same Rodionov regime shift criteria (red and blue solid lines in Fig. 1), in which the mean TC genesis frequency in P2 is significantly reduced in comparison with P1 (Liu and Chan 2013; Choi et al. 2015; He et al. 2015; Zhang et al. 2018; Zhao and Wang 2019). To further investigate the relationship between the PDO index and WNP TC genesis frequency on a low-frequency time scale, we conducted an 11-year running mean of WNP TC genesis frequency and the PDO index. The results indicate that the two indices are closely related (r = 0.67) and their quantities simultaneously changed from positive to negative around 1997/98 (figure not shown), supporting the results of the regime shift algorithm.

A total of 553 TCs developed over the WNP during the analysis period, 306 (~ 56%) during P1 and 247 (~ 44%)

during P2, showing that the TC genesis frequency is significantly reduced by approximately 3.69 per year at the 99% confidence level with a PDO phase shift from positive to negative (Table 1). In addition, we use the TC genesis density to further investigate the regional spatial features of this reduction between both periods (Fig. 2); strong negative genesis anomalies occurred over the eastern WNP, and a mix of negative and positive genesis anomalies occurred over the western WNP (division defined by the 140° E longitude line). To test the sensitivity of these results, we reduce the resolution monotonically from 5° to 2°, and find that the major patterns are insensitive to resolution. We then investigate the mean TC genesis frequency over the total, western, and eastern WNP in both dominant PDO phases (Table 1). The mean TC genesis frequency over the western WNP insignificantly decreased by approximately 6% from P1 to P2, while that over the eastern WNP significantly decreased by ~ 34% at the 99% confidence level (Table 1). Moreover, the correlation on a low-frequency time scale between the western WNP TC genesis frequency and the PDO index is 0.24, which is insignificant, while the eastern WNP TC genesis frequency is highly correlated with the PDO index (r = 0.88), which is significant at the 99% confidence level. The above results imply that the significant reduction in total TC genesis frequency over the WNP between P1 and P2 is primarily caused by a localized reduction over the eastern WNP rather than by a decrease over the entire region (e.g., Zhang et al. 2018). Therefore, hereafter we focus on the reduction of TC genesis frequency in the eastern WNP rather than over the whole WNP.

Table 1 Annual mean TC genesis frequency over the total, western, and eastern parts of the WNP (divided by 140° E longitude, during both PDO phases

	Total	Western	Eastern
Whole period (1982–2013)	17.28 (553)	9.75 (312)	7.53 (241)
P1 (1982–1997)	19.13 (306)	10.06 (161)	9.06 (145)
P2 (1998–2013)	15.44 (247)	9.44 (151)	6.00 (96)
P2–P1	− 3.69*	− 0.62	− 3.06*

Total TC numbers are given in parentheses

*Significance at a 99% confidence level

Fig. 2 TC genesis density (5° by 5°) difference between P2 (negative PDO; 1998–2013) and P1 (positive PDO; 1982–1997). Solid and dashed lines represent regions that are statistically significant at the 95% confidence level

TC genesis density (P2 − P1)
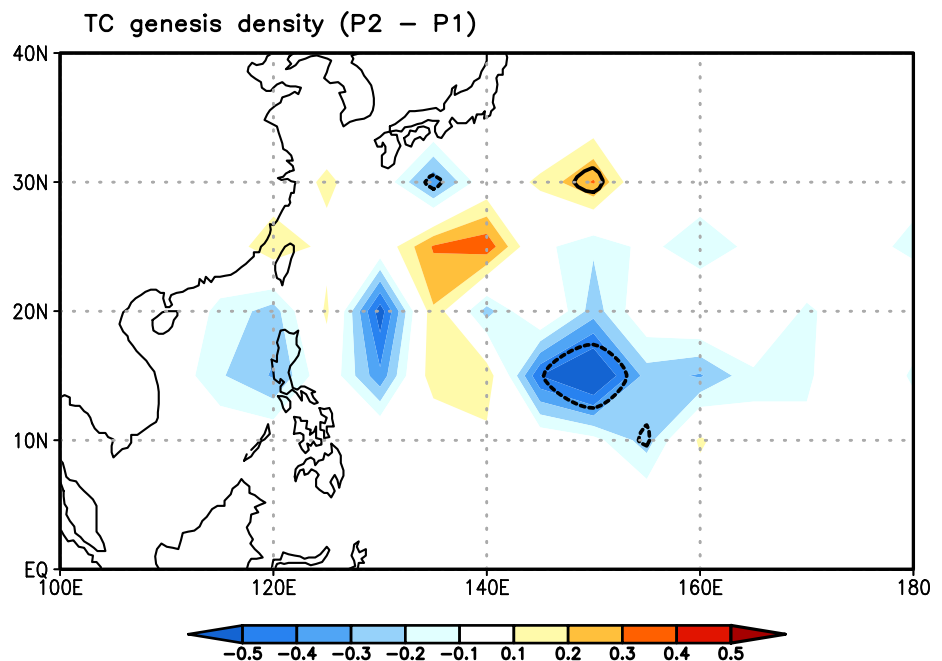
3.2 Relationship between CP ENSO and TC genesis frequency over the eastern WNP

During P1, the maximum interannual standard deviation of the SST anomalies located over the EP (Fig. 3a) and the eastern WNP TC genesis frequency do not show a significant relationship with SST anomalies in the tropical Pacific region (Fig. 3c). In contrast, large interannual variations in SST anomalies developed in the CP (Fig. 3b) in P2. The important thing is that the CP SST anomalies are highly correlated with eastern WNP TC genesis frequency during P2 (Fig. 3d; Zhao and Wang 2019). Taking these considerations into account, we investigate the dynamic mechanisms of CP SST variability modulating the TC genesis frequency over the eastern WNP during P2. For this investigation, we use the Niño-4 index as CP SST anomalies averaged over [5° S to 5° N, 160° E to 150° W] and divided into warm and cold CP phases using its standard deviation thresholds of 0.75 and − 0.75, respectively. The selected warm and cold CP phase corresponded to 4 (2002, 2004, 2006, and 2009) and 6 (1998, 1999, 2000, 2008, 2010, and 2011) years, respectively. This Niño-4 index is more highly correlated with eastern WNP TC genesis frequency during P2 (r = 0.71) than during P1 (r = 0.27), which corresponds to the results in

Fig. 3c, d; however, western WNP TC frequency shows no significant relationship during any period (Table 2).

The strong correlation between the Niño-4 index and TC genesis frequency over the eastern WNP in P2 can be interpreted as a dynamical process related to CP SST variability. The eastern WNP TC genesis frequency is significantly enhanced by the warm CP phase during P2 at the 95% confidence level (Table 3). The increase in eastern WNP TC genesis frequency during the warm CP phase resulted from a Rossby wave response to a warm SST anomaly over the CP region (Fig. 4a, c) that appears in off-equatorial regions of both hemispheres, consistent with a Gill-type response (Gill 1980). This response generates low-level cyclonic

Table 2 Correlation coefficients between the Niño-4 index and total, western, and eastern WNP TC genesis frequency during each analysis period

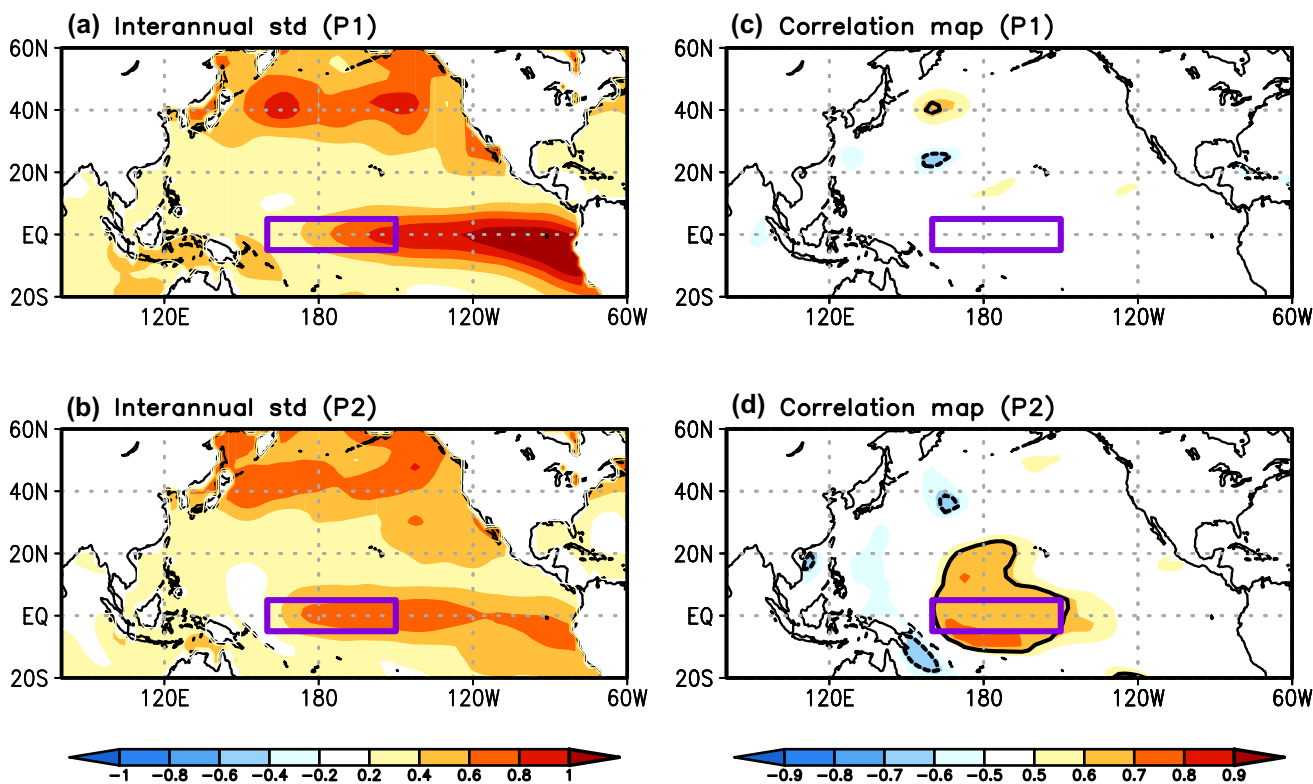|	Total	Western	Eastern
Whole period	0.21	− 0.37	0.46*
P1	0.05	− 0.29	0.27
P2	0.40	− 0.51	0.71*

*Significance at a 99% confidence level

Fig. 3 Interannual standard deviation in SST anomalies (shaded, °C) during **a** P1 (positive PDO; 1982–1997) and **b** P2 (negative PDO; 1998–2013). Correlation map between SST anomalies and eastern WNP TC frequency in **c** P1 and **d** P2. Solid and dashed lines in (**c**) and (**d**) represent regions that are statistically significant at the 99% confidence level. Purple boxes delineate the CP index area

Table 3 Annual mean TC genesis frequency over the eastern WNP for each normalized magnitude by the Niño-4 index in the negative PDO phase (1998–2013)

	Warm	Cold	Total
# of years	4	6	16
Mean frequency	**8.25 (+)**	**3.33 (− −)**	6.00

Warm (cold) corresponds to a normalized index larger (smaller) than 0.75 (− 0.75).The bold font denotes frequencies statistically enhanced (reduced) at the 90% and 95% confidence levels, noted by + and + +(– and – –), respectively

circulation and a negative geopotential height (GPH) anomaly over the northwest of the cold SST forcing (i.e., eastern WNP), leading to significant enhancement of TC genesis frequency over the eastern WNP (Table 3; Fig. 4a, c; Chen and Tam 2010; Kim and Seo 2016).

On the other hand, TC genesis frequency over the eastern WNP is significantly reduced by the cold CP phase at the 95% confidence level during P2 (Table 3). The decrease in eastern WNP TC genesis frequency is also due to the Rossby wave response to the cold SST anomaly over the CP region (Fig. 4c). As a result, the positive GPH anomaly and anticyclonic circulation are located over the eastern WNP

(Fig. 4d), suppressing the TC genesis frequency in this basin (Kim and Seo 2016). In summary, the Rossby wave response induced by the CP SST anomaly is mainly concentrated in the eastern WNP (Fig. 4c, d) during P2, which well corresponds to a significant relationship between CP SST and eastern WNP TC genesis frequency (Table 3).

3.3 Asymmetric CP ENSO frequency and reduction in TC genesis frequency over the eastern WNP

As discussed, the cold (warm) CP phase significantly reduces (enhances) eastern WNP TC genesis frequency (Table 3) by anticyclonic (cyclonic) circulation and the positive (negative) GPH anomaly induced by a Gill-type response on an interannual time scale. Therefore, if the frequency of cold and warm CP phases is asymmetrically regulated by the negative PDO phase during P2, asymmetric CP ENSO frequency plays a crucial role in modulating eastern WNP TC frequency during that period.

From the perspective of asymmetric CP ENSO frequency, our results show that the number of cold CP phases (6) is 50% larger than the number of warm CP phases (4) during P2 (Table 4), in line with results of Lin et al. (2018). In addition, the number of cold phases (6) when using the Niño-3.4
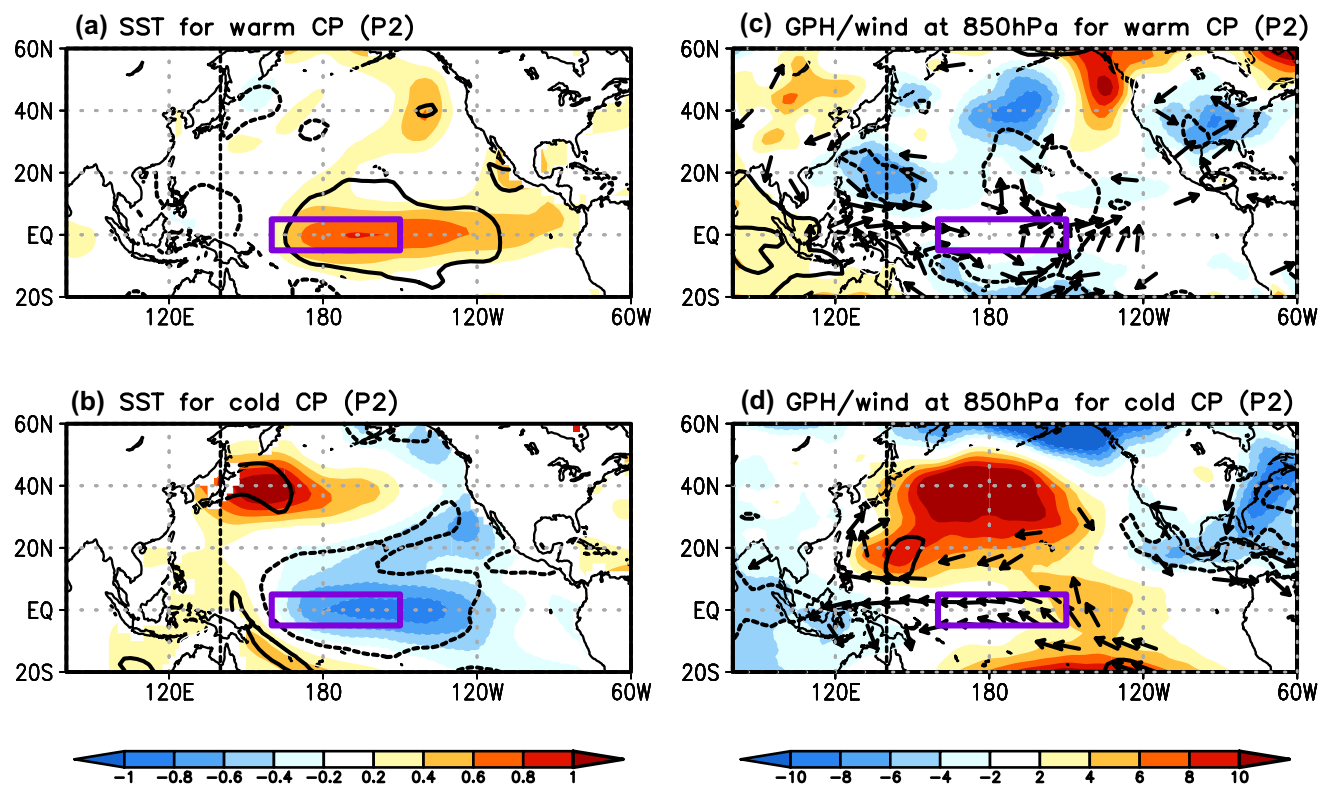

Fig. 4 Composite of SST anomalies (shaded, °C) for **a** 4 warm CP years and **b** 6 cold CP years during P2 (negative PDO; 1998–2013); **c** and **d** are the same as (**a**) and (**b**) except for 850-hPa GPH (shaded, m) and wind (vector, m s⁻¹) anomalies, respectively. Solid and dashed lines represent regions that are statistically significant at the 95% confidence level. Purple box delineates the Niño-4 area

Table 4 Number of warm and cold phases for the three Niño indices during P2

	Niño-4	Niño-3.4	Niño-3
Warm	4 (1)	3 (1)	3 (1)
Cold	6 (6)	6 (5)	3 (2)

Warm (cold) corresponds to a normalized index larger (lower) than 0.75 (− 0.75). Number of warm and cold phases in P2 excluding neutral years of negative PDO are given in parentheses

Table 5 Number of warm and cold phases for the three Niño indices during P1

	Niño-4	Niño-3.4	Niño-3
Warm	4 (2)	4 (3)	4 (3)
Cold	5 (2)	1 (1)	4 (2)

Warm (cold) corresponds to a normalized index larger (lower) than 0.75 (− 0.75). Number of warm and cold phases in P1 excluding neutral years of positive PDO are given in parentheses

index is more than two times larger than the number of warm phases (3), while the Niño-3 index is divided into an equal number of cold and warm phases (3) during P2 (Table 4). It is important to note that we exclude neutral years of the negative PDO, while the frequency of warm and cold phases shows a striking difference. Considering that the normalized PDO index is less than − 0.3 in P2 for excluded neutral years of the negative PDO, only 1 year (2006) is selected as the warm CP phase, while the cold CP phases remain unchanged. In common with the Niño-4 index, the Niño-3.4 index is divided into only one warm phase and five cold phases, however; one warm phase and two cold phases are selected by using the Niño-3 index (Table 4). The results indicate that asymmetric CP ENSO frequency in P2 acts as driving factor for the reduction in TC genesis frequency over the eastern WNP; the asymmetric frequency only appears on CP ENSO related indices, which may reflect the large interannual CP SST variation during P2 (Fig. 3b).

Frequency of warm and cold phases is also calculated using the three Niño indices during P1 to investigate whether the asymmetric frequency is regulated by the positive PDO phase. As a result, 4 (5) years are selected as the warm (cold) CP phases. Moreover, when the neutral years of positive PDO (the normalized PDO index is larger than 0.3) are excluded, an equal number of warm and cold CP phases (2) can be identified (Table 5). However, the Niño-3.4 index is divided into more frequent warm phases than cold phases while including and excluding neutral years of the positive PDO (Table 5). The Niño-3 index has more frequent warm phases than cold phases when excluding neutral years of the positive PDO (Table 5). Asymmetric CP ENSO frequency does not appear in the positive PDO phases, whereas EP ENSO related indices show asymmetric frequency when

excluding neutral years of positive PDO; this may be attributed to the large interannual EP SST variation during that period (Fig. 3a).

To supplement the small number of CP ENSO phases in observations, we use a long-term simulation model to identify this asymmetric CP ENSO frequency in both PDO phases. For this purpose, we first evaluate the performance of the simulated PDO by applying the method suggested by Mantua et al. (1997). This method derived the leading principal component (PC) of monthly SST anomalies in the North Pacific, poleward of 20° N. As a result, the spatial pattern of the simulated PDO is found to correspond well with the observations (Fig. 5a). The yearly PDO index is calculated as the JASO average from the leading PC (Fig. 5b). To exclude neutral years of the PDO, we divide this index into positive and negative phases using a threshold of ± 0.3. As a result, during the 500-year simulation period, there are 206 (182) negative (positive) PDO phases.

To investigate the asymmetric CP ENSO frequency in our long-term simulation model, we use a JASO mean SST anomaly that has a removed regression pattern with the Niño-1 + 2 [over 10° S to 0°, 90° to 80° W] for driving out CP ENSO and eliminating EP ENSO (Yu and Kim 2010; Kim and Yu 2012). We take the simulated Niño-4 index over same area, and then warm and cold CP phases are selected using standard deviation thresholds of 0.75 and − 0.75, respectively.

During negative PDO phases, cold CP phases (50) occur more than warm CP phases (31), and the asymmetric CP ENSO frequency in the simulation model is well matched by our observational results (Fig. 6). The simulated CP ENSO is characterized by shifting a little to the tropical western Pacific (Fig. 7; Deser et al. 2006) compared with the observational CP ENSO (Fig. 4a, b), while the positive (negative) SST anomaly over the mid-latitude northwestern Pacific matches well the observational result in the negative (positive) PDO phase (Fig. 7). Even though we do not detect TCs in the simulation model owing to the resolution, more frequent cold CP phases than warm CP phases can lead to a reduction in TC genesis over the WNP in the model simulation.

In contrast, during positive PDO phases, the number of warm CP phases (50) is larger than the number of cold CP phases (32), so that the TC genesis frequency may be increased by the asymmetric CP ENSO frequency in the simulation model. As we only consider asymmetric CP ENSO by the positive PDO phase in the simulation model, the above results cannot be used in P1 owing to the dominant EP ENSO in that period. The PDO phase changed from negative to positive in and after 2014; as such, if CP ENSO is dominant in the near future, eastern WNP TC genesis frequency is likely to be increased by the asymmetric CP ENSO frequency in the positive PDO phase.

Fig. 5 a Leading empirical orthogonal function mode of north Pacific SST anomalies (shaded, °C) and **b** the yearly PDO index using a long-term CCSM3 simulation model. Red (blue) dashed lines in (**b**) denote standard deviation thresholds of 0.3 (− 0.3)
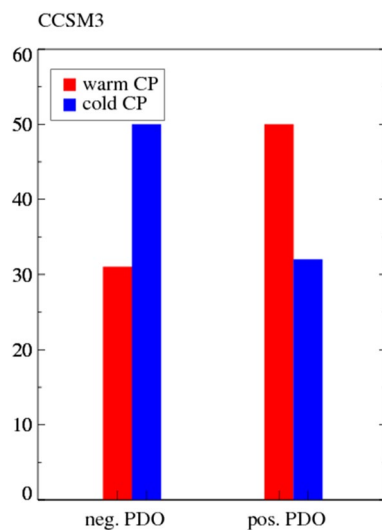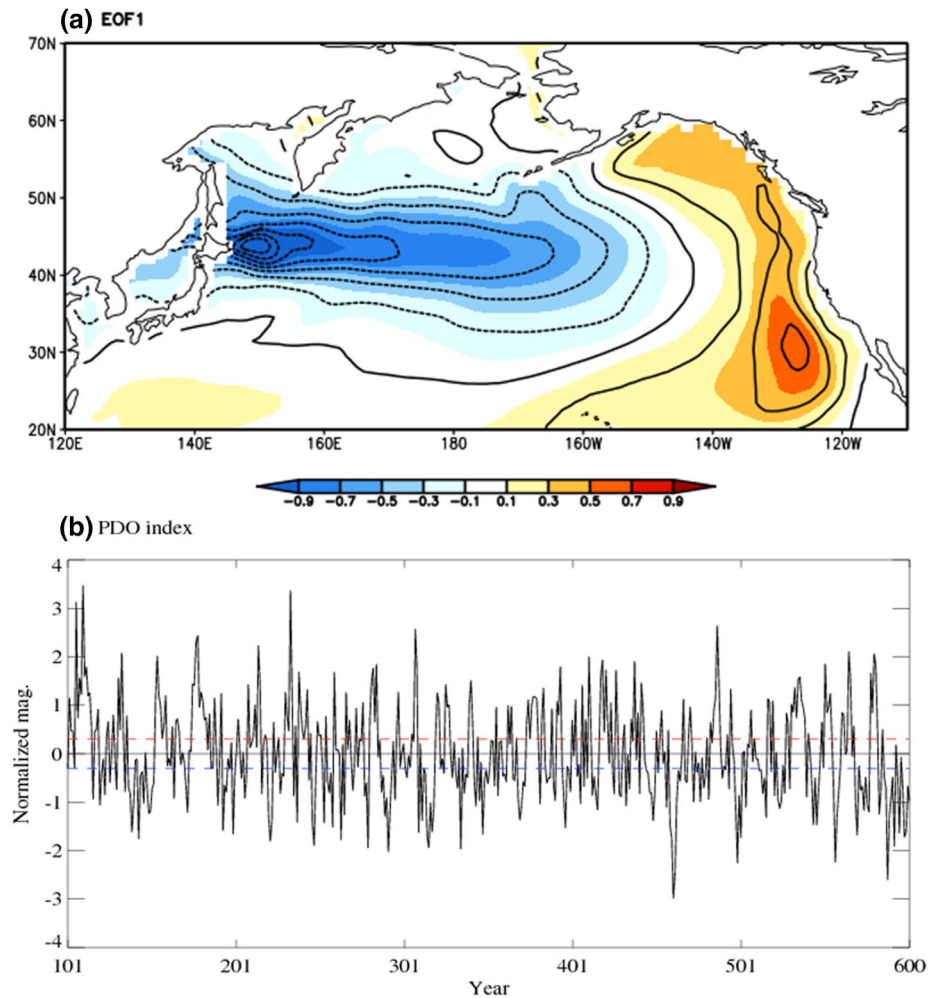

Fig. 6 Frequency of warm (red) and cold (blue) CP phases in both PDO phases using a long-term CCSM3 simulation model

3.4 Asymmetric CP ENSO intensity and reduction in TC genesis frequency over the eastern WNP

From Table 3, the genesis ratio of the eastern WNP TC is increased (decreased) in warm (cold) CP phases during P2. Therefore, if cold (warm) CP phases are relatively stronger (weaker) in P2 than in P1, the genesis ratio of eastern WNP TC is modulated by the asymmetric CP ENSO intensity. As a result, this asymmetric CP ENSO intensity can regulate the TC genesis frequency over the eastern WNP in P2.

To identify the asymmetric intensity of warm and cold CP phase between P2 and P1, composite difference analysis is used. The warm and cold CP phases in P1 are also selected using standard deviation Niño-4 index thresholds of larger than 0.75 and less than − 0.75, respectively. Although the composite difference in SST anomalies in the warm CP phase between P2 and P1 slightly resembles the negative PDO phase, the center of the tropical cold SST anomalies is in the tropical EP region (Fig. 8a) and is due to the large interannual variation of SST anomalies over the tropical EP during P1 (Fig. 3a). Owing to the negative SST anomalies
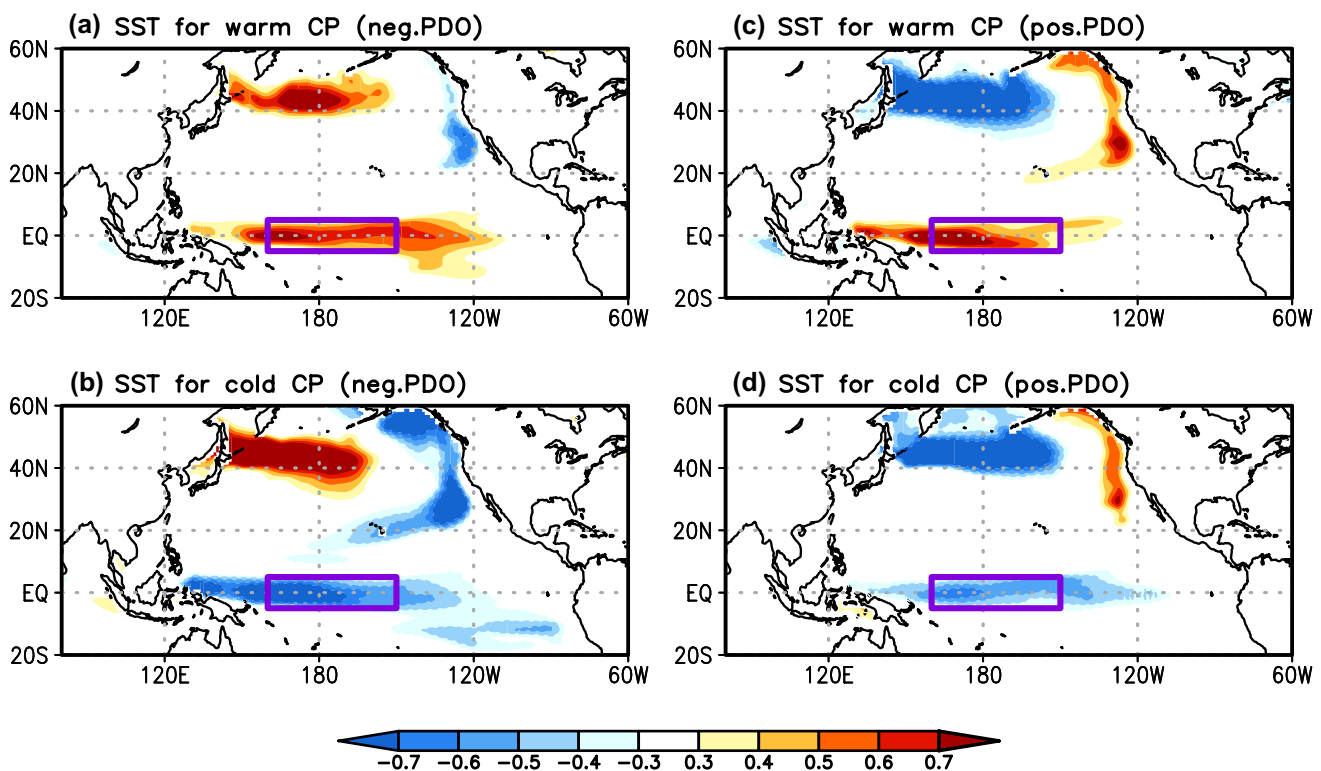
Fig. 7 Composite of SST anomalies (shaded, °C) for **a** 31 warm CP phases and **b** 50 cold CP phases during negative PDO phases using a long-term CCSM3 simulation model; **c** and **d** are the same as (**a**) and (**b**) except for 50 warm CP phases and 32 cold CP phases during positive PDO phases. Purple boxes delineate the Niño-4 area

over the tropical EP (Fig. 8a), negative GPH anomalies are located over the WNP basin through Walker circulation (Fig. 8c).

Compared with the warm CP phase, the composite difference in SST anomalies in the cold CP phase between P2 and P1 shows cold SST anomalies in the tropical CP and warm SST anomalies in the mid-latitude northwestern Pacific, corresponding roughly with SST patterns for the negative PDO phase (Fig. 8b). The negative SST anomaly over the tropical CP implies that cold CP phases are stronger in P2 than in P1 (Fig. 8b). In addition, the negative SST anomaly over the CP region is evidence of asymmetric CP ENSO frequency when using Niño-4 and Niño-3.4, but not when using Niño-3 as previously discussed. On this basis, we can expect that the Gill-type response induced by cold CP phases has a stronger intensity in P2 than in P1. Figure 8d shows the composite difference of the cold CP phase in GPH and wind vector anomalies at 850-hPa between P1 and P2. A significant positive GPH anomaly and anticyclonic circulation are located over the eastern WNP (Fig. 8d), which come from the stronger intensity Gill-type response in P2 than in P1 due to the stronger cold CP phases in P2 than in P1. This large-scale atmospheric circulation pattern increases the reduction

ratio for eastern WNP TC genesis (Table 3), suppressing TC genesis frequency in the basin.

To underpin the asymmetric CP ENSO intensity of the observational data, the asymmetric CP ENSO intensity in the long-term simulation model is also investigated by composite difference analysis. The composite difference patterns of SST anomalies and GPH/wind anomalies at 850-hPa in cold CP phases between the negative and positive PDO phases are similar to the observational results (Fig. 9b, d); however, the simulated negative SST anomaly is located over the Philippine Sea, which is a slight shift to the northwestward compared with the observed negative tropical CP SST anomaly. Owing to the shifted negative SST anomaly, the positive GPH anomaly and anticyclonic circulation induced by the Gill-type response is more westerly than that of the observational results (Fig. 9d). Therefore, in model simulation, these atmospheric circulations can increase the reduction ratio for TC genesis, reducing TC genesis over the WNP basin.

In addition, the composite difference in the SST anomalies and GPH/wind anomalies at 850-hPa in warm CP phases between negative and positive PDO phases slightly differ from the observational results (Fig. 9a, c); this is partly due to only CP ENSO in the simulation model. However,
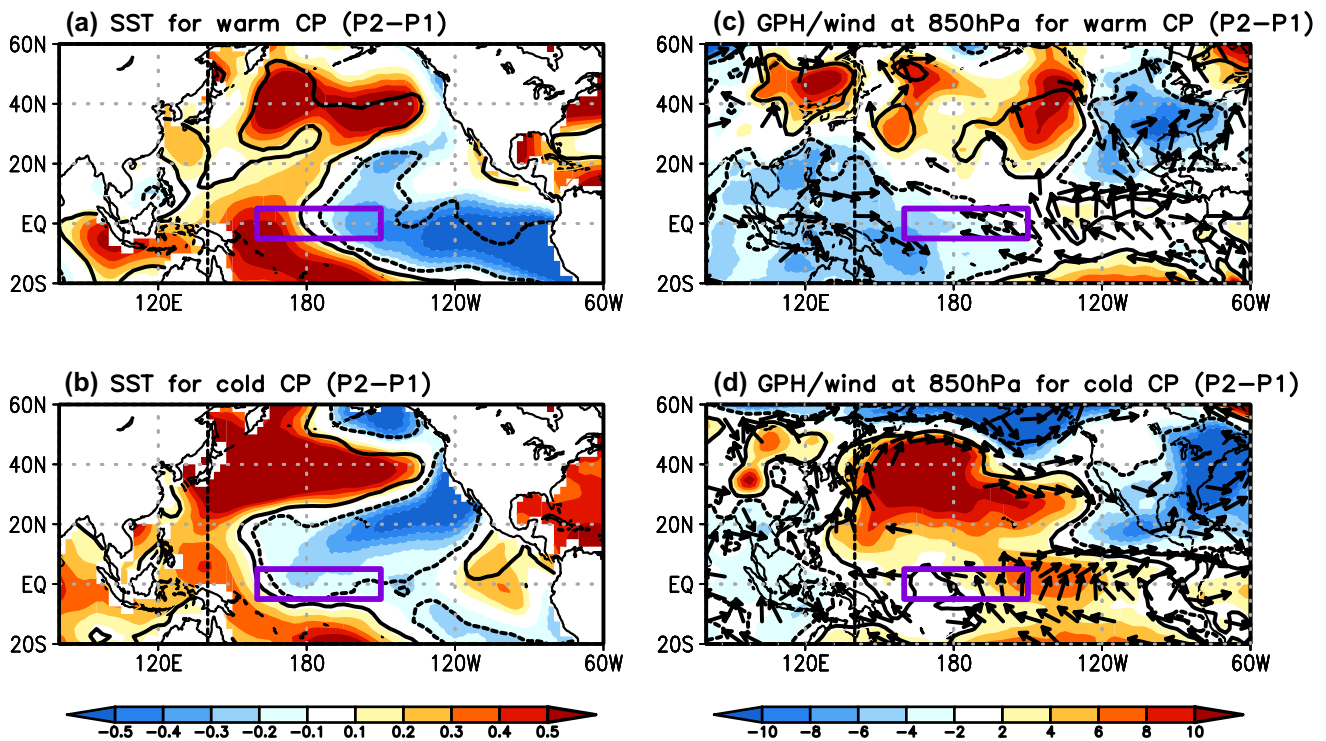
Fig. 8 Composite difference of SST anomalies (shaded, °C) in **a** warm CP years and **b** cold CP years between P2 (negative PDO; 1988–2013) and P1 (positive PDO; 1982–1997); **c** and **d** are the same as (**a**) and (**b**) except for 850-hPa GPH (shaded, m) and wind (vec-

tor, m s^{-1}) anomalies, respectively. Solid and dashed lines represent statistical significance at the 95% confidence level. Vectors are significant at the 95% confidence level. Purple boxes delineate the Niño-4 area

the simulated results offer indirect evidence that warm CP phases and their Gill-type response during a negative PDO phase are weaker than during positive PDO phases, resulting in a decrease in the enhancement ratio and suppression of TC genesis.

4 Summary and discussion

Compared with P1, P2 mean TC genesis frequency over the WNP is significantly reduced by approximately 19% (Table 1). This significant reduction primarily results from a decrease in TC genesis frequency over the eastern WNP (Fig. 2; Table 1). In addition, the relationship between the eastern WNP TC genesis frequency and CP SST anomalies becomes more intense in P2 than in P1 (Table 2). To explain these phenomena, we apply the asymmetric CP ENSO properties induced by a negative PDO phase. In other words, the frequent cold CP phases and less frequent warm CP phases decrease the eastern WNP mean TC genesis frequency in P2. Furthermore, the stronger cold CP phases in P2 compared with P1 intensify the reduction amount for TC genesis frequency over the eastern WNP, inducing a lower frequency of TC genesis.

Many previous studies have suggested that the significant reduction in WNP TC genesis frequency following PDO phase-shifting is caused by intensification of vertical wind shear by the negative PDO-induced cold SST anomalies and easterly wind anomalies over the tropical Pacific on a decadal time scale (e.g., Liu and Chan 2013; Zhang et al. 2018; Zhao and Wang 2019). Similarly, the asymmetric CP ENSO properties can be the main cause of the intensification of vertical wind shear during P2. In other words, more frequent and stronger cold CP phases are concurrent with more frequent and stronger low-level easterly wind anomalies during P2, while weaker low-level westerly wind anomalies are accompanied by less frequent and weaker warm CP phases; as such, easterly wind anomalies dominate in P2, leading to intensification of vertical wind shear.

We also investigate the asymmetric CP ENSO properties by both PDO phases using the pre-industrial CMIP5 model experiments, including GFDL-CM3 (200 years) and CNRM-CM5 (160 years). As a result, the main conclusions are consistent with the CCSM3 simulation results (Table 6). The asymmetric CP ENSO properties may be due to mean state changes in different PDO phases. During the negative PDO phase, anomalous easterly winds dominate in the tropical Pacific, potentially playing a role in frequent and intense
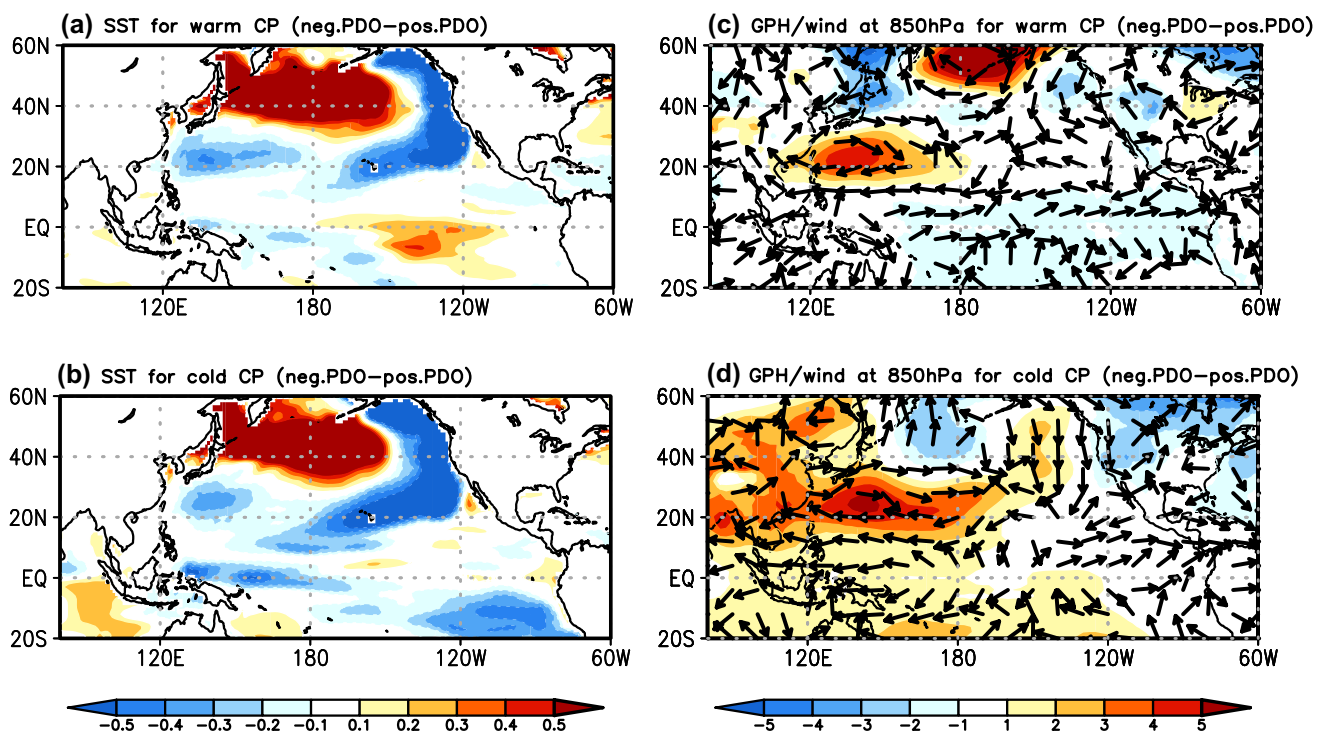
Fig. 9 Composite difference of simulated SST anomalies (shaded, °C) in **a** warm CP phases and **b** cold CP phases between negative PDO and positive PDO; **c** and **d** are the same as (**a**) and (**b**) except for simulated 850 hPa GPH (shaded, m) and wind (vector, m s^{-1}) anomalies, respectively. Purple boxes delineate the Niño-4 area

Table 6 Number of warm and cold CP phases in both PDO phases using GFDL-CM3 (200 years) and CNRM CM5 (160 years) simulation models

GFDL/CNRM	Negative PDO	Positive PDO
Warm	11/8	28/20
Cold	24/12	11/7

Positive and negative PDO phases are divided as having a normalized PDO index larger than 0.3 and lower than −0.3, respectively. Warm (cold) corresponds to a normalized Niño-4 index larger (lower) than 0.75 (−0.75)

La Niña events; the reverse may also be true. Therefore, for example, westerly wind bursts (Eisenman et al. 2005) may cause CP ENSO asymmetry; this will be a focus of future research using daily-scale long-term simulation models.

The TC genesis frequency in P1 also demonstrates a nonlinear relationship with both CP ENSO phases. Kim and Seo (2016) showed that warm CP phases provide favorable conditions through their Gill-type response for eastern WNP TC genesis frequency, whereas atmospheric conditions over the main WNP TC development region during cold CP phases are similar to average years; in P1, this may be due to the weak intensity of cold CP. However, during this period, Walker circulation also plays an important role

in modulating TC genesis frequency over the western WNP because EP SST variation dominates.

Previous studies have shown that the Atlantic SST variability on the interannual and decadal time scales is a key driver of the WNP TC activity and CP ENSO. For example, Yu et al. (2016) investigated the effects of tropical North Atlantic SST on the WNP TC genesis frequency in the interannual time scale. They found a significant negative relationship between WNP TC genesis frequency and tropical North Atlantic SST anomalies. This relationship resulted from the combined effect of air-sea interaction and Gill-type response from the tropical North Atlantic to the eastern WNP and Indian Ocean. In addition, on a decadal time scale, the AMO can also modulate WNP TC genesis frequency; however, very few studies have investigated this relationship (e.g., Zhang et al. 2018). Yu et al. (2015) showed that the intensification of Pacific meridional mode in the early 1990s provides favorable conditions for the development of CP El Niño. This intensification is associated with strengthening of the subtropical Pacific high caused by a phase change of the AMO. Therefore, impact of the Atlantic SST variability including AMO on WNP TC genesis frequency via modulation of CP ENSO merits further investigation.

Di Lorenzo et al. (2010, 2015) showed the linkage mechanism between NPGO and CP ENSO; the CP

ENSO is an important factor modulating the TC genesis frequency in the eastern part of the WNP. Therefore, the eastern WNP TC genesis frequency may be controlled by NPGO. From correlation analysis, we identified a significant relationship between the NPGO index and the genesis frequency of TC over the entire WNP on a low-frequency time scale (11-year running mean of both indices; r = − 0.93), in line with the results of Zhang et al. (2013). In addition, the eastern and western WNP TC genesis frequencies are also highly correlated with the NPGO index (r = − 0.94 and −0.68, respectively) on a low-frequency time scale, suggesting a distinct impact of PDO and NPGO on TC genesis frequency. The current study mainly focuses on the impact of asymmetric CP ENSO properties on eastern WNP TC genesis frequency. Therefore, if the properties of CP ENSO are asymmetrically regulated by both NPGO phases, the latter can be considered an important driver for the significant reduction of the eastern WNP TC genesis frequency. For this reason, we investigate the asymmetric frequency and intensity of CP ENSO associated with both NPGO phases using the long-term CCSM3 simulation model. As per the obtained results, the frequency and intensity of CP ENSO are similar in both NPGO phases. Therefore, NPGO may not modulate TC genesis frequency from the viewpoint of the asymmetric CP ENSO properties.

Zhao et al. (2019a) found that the interannual relationship between the WNP summer monsoon and WNP TC genesis frequency has intensified since 1998 with a significant reduction of TC genesis frequency in the WNP monsoon trough region. They showed that these changes resulted from the ENSO shifting from EP to CP since the late 1990s, with PDO phase transition from positive to negative. In addition, ENSO shifting from EP to CP also induces change in the interannual relationship between WNP TC cyclogenesis latitude and longitude (Zhao et al. 2019b). That is to say, increasing occurrence in CP ENSO events since the late 1990s led to a west-northward or south-eastward shift of WNP tropical cyclogenesis location. In this context, the above proposed relationships are may regulated by asymmetric CP ENSO properties.

This study focuses on the relationships between eastern WNP TC genesis frequency and CP SST variation during a negative PDO phase. The PDO phase slowly shifted from negative to positive in and after 2014; if high CP SST variation continues to dominate, then, eastern WNP TC genesis frequency may increase in the near future because of the relationship between the positive PDO phase and asymmetric CP ENSO properties. The findings of this research can be applied to TC prediction models over the WNP, which will be the subject of future research.

References

An S-I (2018) Impact of Pacific Decadal Oscillation on frequency asymmetry of El Niño and La Niña events. Adv Atmos Sci 35(5):493–494. https://doi.org/10.1007/s00376-018-8024-7

Camargo SJ, Emanuel KA, Sobel AH (2007) Use of a genesis potential index to diagnose ENSO effects on tropical cyclone genesis. J Clim 20:4819–4834. https://doi.org/10.1175/JCLI4282.1

Chan JCL (2008) Decadal variations of intense typhoon occurrence in the western North Pacific. Proc R Soc A 464:249–272

Chen GH, Tam CY (2010) Different impacts of two kinds of Pacific Ocean warming on tropical cyclone frequency over the western North Pacific. Geophys Res Lett 37:L01803. https://doi.org/10.1029/2009GL041708

Choi YM, Ha K-J, Ho C-H, Chung CE (2015) Interdecadal change in typhoon genesis condition over the western North Pacific. Clim Dyn 45:3243–3255

Collins WD et al (2006) The community climate system model version 3 (CCSM3). J Clim 19:2122–2143. https://doi.org/10.1175/JCLI3761.1

Deser C, Capotondi A, Saravanan R, Phillips A (2006) Tropical Pacific and Atlantic variability in CCSM3. J Clim 19:2451–2481

Di Lorenzo E, Cobb KM, Furtado JC, Schneider N, Anderson BT, Bracco A, Alexander MA, Vimont DJ (2010) Central Pacific El Niño and decadal climate change in the North Pacific Ocean. Nat Geosci. https://doi.org/10.1038/NGEO0984

Di Lorenzo E, Liguori G, Schneider N, Furtado JC, Anderson BT, Alexander MA (2015) ENSO and meridional modes: a null hypothesis for Pacific climate variability. Geophys Res Lett 42:9440–9448

Eisenman I, Yu L, Tziperman E (2005) Westerly wind bursts: ENSO's tail rather than the dog? J Clim 18:5224–5237. https://doi.org/10.1175/JCLI3588.1

Gill AE (1980) Some simple solutions for heat-induced tropical circulations. Q J Roy Meteor Soc 106:447–462. https://doi.org/10.1002/qj.49710644905

He H, Yang J, Gong D, Mao R, Wang Y, Gao M (2015) Decadal changes in tropical cyclone activity over the western North Pacific in the late 1990s. Clim Dyn 45:3317–3329

Hsu PC, Chu PS, Murakami H, Zhao X (2014) An abrupt decrease in the late-season typhoon activity over the western North Pacific. J Clim 27:4296–4313

Huang B, Banzon VF, Freeman E, Lawrimore J, Liu W, Peterson TC, Smith TM, Thorne PW, Woodruff SD, Zhang HM (2014) Extended reconstructed sea surface temperature version 4 (ERSST.v4): Part I. Upgrades and intercomparisons. J Clim 28:911–930. https://doi.org/10.1175/JCLI-D-14-00006.1

Jin C-S, Ho C-H, Kim J-H, Lee D-K, Yeh S-W (2013) Impact of central Pacific El Niño on tropical cyclone tracks over the East China Sea using WRF-based global and regional climate model. J Clim 26:2534–2545

Kalnay E, Kanamitsu M, Kistler R, Collins W, Deaven D, Gandin L, Iredell M, Saha S, White G, Woollen J, Zhu Y, Chelliah M, Ebisuzaki W, Higgins W, Janowiak J, Mo KC, Ropelewski C, Wang J, Leetmaa A, Reynolds R, Jenne R, Joseph D (1996) The NCEP/NCAR 40-year reanalysis project. Bull Amer Meteorol Soc 77:437–471. https://doi.org/10.1175/1520-0477(1996)077%3c0437:TNYRP%3e2.0.CO;2

Kao H-Y, Yu J-Y (2009) Contrasting Eastern-Pacific and Central-Pacific types of ENSO. J Clim 22:615–632. https://doi.org/10.1175/2008JCLI2309.1

Kim H-K, Seo K-H (2016) Cluster analysis of tropical cyclone tracks over the western North Pacific using a self-organizing map. J Clim 29:3731–3751. https://doi.org/10.1175/JCLI-D-15-0380.1

Kim ST, Yu J-Y (2012) The two types of ENSO in CMIP5 models. Geophys Res Lett 39:L11704. https://doi.org/10.1029/2012GL052006

Li RCY, Zhou W (2013a) Modulation of western North Pacific tropical cyclone activity by the ISO. Part I: Genesis and intensity. J Clim 26:2904–2918. https://doi.org/10.1175/JCLI-D-12-00210.1

Li RCY, Zhou W (2013b) Modulation of Western North Pacific tropical cyclone activity by the ISO. Part II: Tracks and landfalls. J Clim 26:2919–2930. https://doi.org/10.1175/JCLI-D-12-00211.1

Lin RP, Zheng F, Dong X (2018) ENSO frequency asymmetry and the Pacific Decadal Oscillation in observations and 19 CMIP5 models. Adv Atmos Sci 35(5):495–506. https://doi.org/10.1007/s00376-017-7133-z

Liu KS, Chan JCL (2013) Inactive period of Western North Pacific tropical cyclone activity in 1998–2011. J Clim 26:2614–2630

Liu Y, Chen GH (2018) Intensified influence of the ENSO modoki on boreal summer tropical cyclone genesis over the western North Pacific since the early 1990s. Int J Climatol. https://doi.org/10.1002/joc.5347

Liu W, Huang B, Thorne RW, Banzon VF, Zhang H-M, Freeman E, Lawrimore J, Peterson TC, Smith TM, Woodruff SD (2015) Extended reconstructed sea surface temperature version 4 (ERSST.v4): Part II. Parametric and structural uncertainty estimations. J Clim 28:931–951. https://doi.org/10.1175/JCLI-D-14-00007.1

Mantua NJ, Hare SR, Zhang Y, Wallace JM, Francis RC (1997) A Pacific interdecadal climate oscillation with impacts on salmon production. Bull Amer Meteor Soc 78:1069–1079

Moon I-J, Kim S-H, Chan JCL (2019) Climate change and tropical cyclone trend. Nature 570:E3–E5

Rodionov SN (2004) A sequential algorithm for testing climate regime shifts. Geophys Res Lett 31:L09204. https://doi.org/10.1029/2004GL019448

Wang B, Chan JCL (2002) How strong ENSO events affect tropical storm activity over the western North Pacific. J Clim 15:1643–1658. https://doi.org/10.1175/1520-0442(2002)015%3c1643:HSEEAT%3e2.0.CO;2

Wang B, Xiang B, Lee J-Y (2013a) Subtropical High predictability establishes a promising way for monsoon and tropical storm prediction. PNAS 110(8):2718–2722

Wang C, Li C, Mu M, Duan W (2013b) Seasonal modulations of different impacts of two types of ENSO events on tropical cyclone activity in the western North Pacific. Clim Dyn 11–12:2887–2902. https://doi.org/10.1007/s00382-012-1434-9

Yeh S-W, Kang S-K, Kirtman BP, Kim J-H, Kwon M-H, Kim C-H (2010) Decadal change in relationship between western North Pacific tropical cyclone frequency and the tropical Pacific SST. Meteorol Atmos Phys 106(3–4):179–189

Yeh S-W, Cai W, Min S-K, McPhaden MJ, Dommenget D, Dewitte B, Collins M, Ashok K, An S-I, Yim B-Y, Kug J-S (2018) ENSO atmospheric teleconnections and their response to greenhouse gas forcing. Rev Geophys 56:185–206. https://doi.org/10.1002/2017RG000568

Yu J-Y, Kim ST (2010) Identification of central-Pacific and eastern-Pacific types of El Niño in CMIP3 models. Geophys Res Lett 37:L15705. https://doi.org/10.1029/2010GL044082

Yu J-Y, Kao P-K, Paek H, Hsu H-H, Hung C-W, Lu M-M, An S-I (2015) Linking emergence of the Central Pacific El Niño to the Atlantic multidecadal oscillation. J Clim 28(2):651–662. https://doi.org/10.1175/JCLI-D-14-00347.1

Yu J, Li T, Tan Z, Zhu Z (2016) Effects of tropical North Atlantic SST on tropical cyclone genesis in the western North Pacific. Clim Dyn 46(3):865–877. https://doi.org/10.1007/s00382-015-2618-x

Zhang W, Leung Y, Min J (2013) North Pacific Gyre Oscillation and the occurrence of western North Pacific tropical cyclones. Geophys Res Lett 40:5205–5211

Zhang W, Vecchi GA, Murakami H, Villarini G, Delworth TL, Yang X, Jia L (2016) The Pacific meridional mode and the occurrence of tropical cyclones in the Western North Pacific. J Clim 29(1):381–398. https://doi.org/10.1175/JCLI-D-15-0282.1

Zhang W, Vecchi GA, Murakami H, Villarini G, Delworth TL, Yang X, Jia L (2018) Dominant role of Atlantic multidecadal oscillation in the recent decadal changes in Western North Pacific tropical cyclone activity. Geophys Res Lett 45:354–362

Zhao H, Wang C (2016) Interdecadal modulation on the relationship between ENSO and typhoon activity during the late season in the Western North Pacific. Clim Dyn 47(1):315–328

Zhao H, Wang C (2019) On the relationship between ENSO and tropical cyclones in the western North Pacific during the boreal summer. Clim Dyn. https://doi.org/10.1007/s00382-018-4136-0

Zhao H, Duan X, Raga GB, Klotzbach PJ (2018) Changes in characteristics of rapidly intensifying western North Pacific tropical cyclones related to climate regime shifts. J Clim 31:8163–8179

Zhao H, Chen S, Klotzbach PJ (2019a) Recent strengthening of the relationship between the Western North Pacific monsoon and Western North Pacific tropical cyclone activity during the Boreal summer. J Clim. https://doi.org/10.1175/JCLI-D-19-0016.1

Zhao H, Zhang J, Klotzbach PJ, Chen S (2019b) Recent increased co-variability of tropical cyclogenesis latitude-longitude over the western North Pacific during the extended boreal summer. J Clim. https://doi.org/10.1175/JCLI-D-19-0009.1